Journal of Colloid and Interface Science 623 (2022) 735–743

Contents lists available at ScienceDirect

Journal of Colloid and Interface Science

journal homepage: www.elsevier.com/locate/jcis

B/N co-doped carbon supported molybdenum carbide catalysts with oxygen vacancies for facile synthesis of flavones through oxidative dehydrogenation

Wen-Ting Chen [a,b], Song Han [a], Zi-Teng Gao [a], Ming-Shuai Sun [a], Zhang-Min Li [a], Duan-Jian Tao [a,*]

[a] Key Laboratory of Fluorine and Silicon for Energy Materials and Chemistry of Ministry of Education, College of Chemistry and Chemical Engineering, Jiangxi Normal University, Nanchang 330022, China
[b] School of Chemical Engineering, Guizhou Institute of Technology, Guiyang 550003, China

HIGHLIGHTS

- B/N co-doped carbon supported Mo_2C catalysts with oxygen vacancies were prepared.
- The oxidative dehydrogenation of flavanones to flavones was performed smoothly.
- The synergistic effect between Mo_2C and oxygen vacancies results in good yields.
- β-Mo_2C can greatly reduce the activation energy of flavanone dehydrogenation.
- O vacancies could activate O_2 with the dissociated H atom to generate ·OH radicals.

GRAPHICAL ABSTRACT

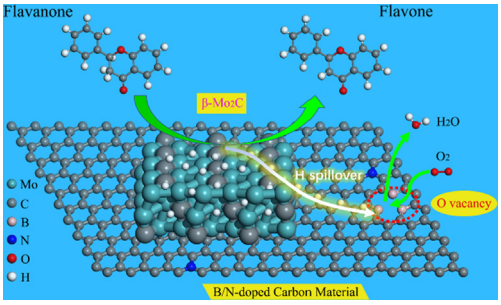

ARTICLE INFO

Article history:
Received 13 April 2022
Revised 8 May 2022
Accepted 14 May 2022
Available online 18 May 2022

Keywords:
Flavones
Oxidative dehydrogenation
Mo_2C
Carbon material
Oxygen vacancy

ABSTRACT

Flavonoids are a type of naturally bioactive molecules, but their chemical producing methods are challenging. Herein, a simple and effective one-step pyrolysis method was developed to successfully prepare a series of molybdenum carbide catalysts dispersed on B and N-codoped carbon materials (Mo_2C@BNC-*x*). Under a calcination temperature of 1000 °C, the as-prepared Mo_2C@BNC-1000 served as a highly efficient heterogeneous catalyst for oxidative dehydrogenation of flavanones into flavones, and the conversion and yield were both 99%. Moreover, several characterizations and density functional theory calculations showed the excellent catalytic performance of Mo_2C@BNC-1000 catalyst originated from the synergistic effect between Mo_2C and the B/N co-doped carbon support with rich oxygen vacancies. In addition, the Mo_2C@BNC-1000 catalyst showed good applicability and reusability, with no significant reduction in catalytic activity at least five runs. The prepared Mo_2C@BNC catalyst thus triggers facile synthesis of flavones through oxidative dehydrogenation of flavanone with green economy and high efficiency.

1. Introduction

Flavones or 2-phenylchromones are one of the most ubiquitous polyphenolic secondary metabolites existing in natural products and their corresponding derived foods. These compounds exhibit a wide range of biological activities, including antidiabetic, antiox-

* Corresponding author.
E-mail address: djtao@jxnu.edu.cn (D.-J. Tao).

https://doi.org/10.1016/j.jcis.2022.05.081
0021-9797/

idant, anticancer, and chemopreventive properties [1]. However, even via high-speed countercurrent chromatography, the content of flavonoids isolated directly from plants in an optimized solvent system remains very low [2,3]. Consequently, the chemical synthesis of flavonoids has become a hot research topic in chemistry and medicine, particularly the development of efficient, clean, and cheap catalysts for their synthesis.

At present, several methodologies for synthesis of flavonoids are reported. The most attractive route is the chalcone route because the 2′-hydroxychalcone intermediates can be readily synthesized by a base-catalyzed Claisen–Schmidt condensation of readily available 2′-hydroxyacetophenones and benzaldehydes [4]. However, the oxidative dehydrogenation of flavanones in the route is still problematic. As illustrated in Scheme 1, a halogen-based oxidant I_2 has to be used and suffers from the drawbacks related to its homogeneous nature and unrecyclability [4,5]. Subsequently, noble metal catalysts have been reported for oxidative dehydrogenation of flavanones by using gold nanoparticles loaded on Mg–Al layered double hydroxide (Au/LDH) [6]; however, the catalytic selectivity of flavone was only 76% and the Au/LDH catalyst was very easily deactivated with a severe loss of catalytic performance after 2 runs. Therefore, a method with excellent atomic economy and heterogeneous efficiency for direct oxidative dehydrogenation of flavanones to flavones is still required.

Previous studies have revealed similarities between the electronic structure of the d orbital in the outer layer of molybdenum carbide (Mo_2C) and the platinum family [7,8]. With high electrical conductivity and optimal hydrogen-adsorption properties, Mo_2C has intensely awakened ever-increasing attention as a nonprecious metal candidate for efficient dehydrogenation [9–12]. However, the limited exposed active sites have brought adverse effects on direct employment of bulk Mo_2C as catalyst [13–15]. Thereby, it is highly anticipated to find an efficient strategy for Mo_2C fabrication and boost its catalytic activity. Prospectively, hetero-atoms (e.g. N, B or others) as dopant into carbon can modulate catalyst's physical and chemical properties to have good catalytic activity and selectivity in the oxidative dehydrogenation (ODH) reactions [16–18]. For example. Wang et al. reported that a codoped boron–nitrogen–carbon-supported (Co—B—N—C) catalyst nanostructure was superior to Co—N—C for the selective oxidation of ethylbenzene [19]. Bordoloi et al. synthesized a mesoporous B_xCN material which displays excellent activity and selectivity in oxidative dehydrogenation of propane [20]. Therefore, a rational design of a hybrid catalyst combing both super properties of Mo_2C and B, N-codoped carbon material is a promising and attractive methodology for oxidative dehydrogenation of flavanone.

Herein, we made an attempt to highly disperse Mo_2C in a nanoscale on B,N-codoped carbon material for efficient oxidative dehydrogenation of flavanones to flavones. A series of heterogeneous Mo_2C-supported B—N—C catalyst (Mo_2C@BNC-*x*) were prepared by simple low-cost raw materials mixing and one-step pyrolysis. The appropriate pyrolysis temperature for the formation of Mo_2C and catalyst endurance were studied. Reaction mechanism of the highly active and selective catalyst was investigated by various characterizations and density functional theory (DFT) calculations.

2. Experimental section

2.1. Materials

Phosphomolybdic acid (96.5%), urea (99%), boric acid (99.5%), *D*-(+)-glucose (98%), flavanone (98%), 5,5-dimethyl-1-pyrroline *N*-oxide (DMPO, 97%),1,4-benzoquinone (98%), ammonium formate (98%), tertiary butanol (99%), butylated hydroxytoluene (99%), and commercialized β-Mo_2C powder (99%) were purchased from Shanghai Macklin Biochemical Co., Ltd. 6-Methoxyflavanone (98%), 4-methoxyflavanone (98%), 6-methylflavanone (98%), 4-methylflavanone (98%), and 2-(4-chlorophenyl)chroman-4-one (98%) were purchased from Adamas-Beta Co., Ltd. The other chemicals were used as purchased without further treatment.

2.2. Preparation of molybdenum carbide catalysts

The Mo_2C@BNC-*x* samples can be synthesized by two steps including mechanical grinding and high temperature calcination. In a typical run, phosphomolybdic acid (1.2 g), boric acid (2.0 g), urea (4.0 g), and D-(+)-glucose (16.0 g) were added into a 50 mL of agate mortar, respectively. Then these four solid components were homogeneously mixed together by vigorous grinding for 10 min. After that, the solid mixture was calcined at 1000 °C for 8 h with a heating rate of 5 °C/min under N_2 atmosphere. The Mo_2C@BNC-1000 sample was finally obtained. For comparison, Mo_2C@BNC-800 and Mo_2C@BNC-900 can be prepared with similar procedures with that of Mo_2C@BNC-1000 by adjusting calcination temperature. The reference catalyst Mo—N—C/1000 was also prepared according to the preparation procedure of Mo_2C@BNC-1000, only excepting the use of raw material boric acid.

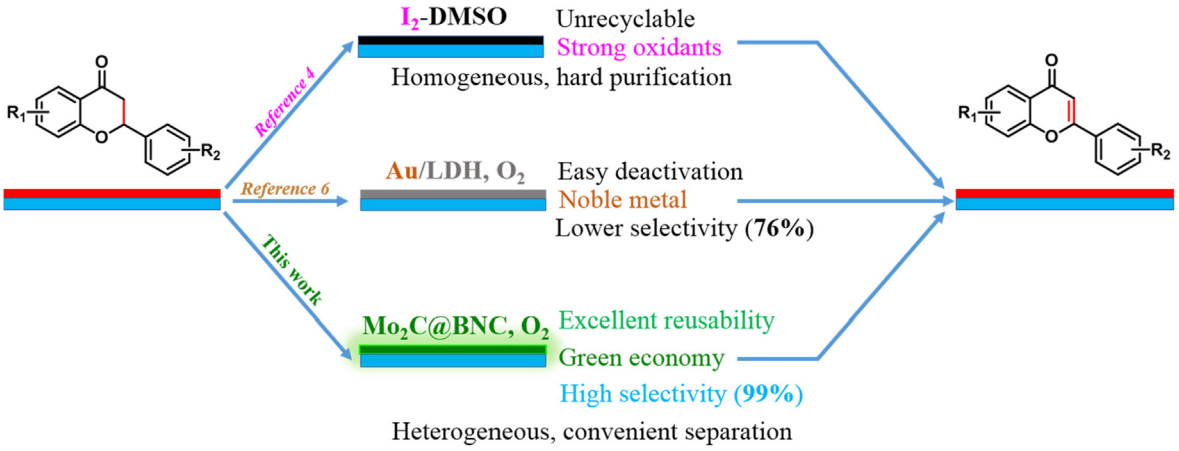

Scheme 1. Synthesis of flavones catalyzed by various catalyst systems.

2.3. Characterization

X-ray diffraction (XRD) patterns of Mo_2C@BNC-*x* were obtained on a Rigaku RINT-2200 diffractometer using a Cu Kα source. Fourier transform infrared (FTIR) spectra were measured by a Nicolet 6700 spectrometer. N_2 adsorption–desorption analysis was carried out by Micromeritics TriStar II 3020 at −196 °C. The morphology and particle size of Mo_2C@BNC-*x* were characterized by field emission scanning electron microscope (SEM, HITACHI S-3400N) and transmission electron microscopy (TEM, JEOL JEM-2100). The surface elemental information was recorded on AXIS Supra X-ray photoelectron spectroscopy (XPS, Kratos Analytical) with an Al Kα radiation source. Electron paramagnetic resonance (EPR) spectra was recorded at room temperature on a Bruker EMXplus-9.5/12 spectrometer. Spin trapping experiments were performed in a reaction mixture containing 100 mmol/L DMPO.

2.4. Catalytic reaction

The oxidative dehydrogenation of flavanone was conducted in a 25 mL stainless steel autoclave. In a typical run, 0.05 g Mo_2C@BNC-1000 catalyst, 0.06 g flavanone, and 6 mL ethanol were added into the batch reactor. And then the reactor was pressured with O_2. Afterward, the reactor was heated to 180 °C for 10 h under 1.8 MPa O_2. After the reaction, the catalyst was first separated from the reaction mixture by filtration. the recycled catalyst was washed with ethanol three times and used for the next run after drying. The liquid products were analyzed qualitatively through gas chromatography-mass spectrometry (GC–MS, 1300 GC-ISQ, Thermo Trace). Quantitative analysis of the liquid products was identified by a gas chromatograph (GC, Thermo Trace 1310) equipped with a capillary column TG-5HT (30 m × 0.25 mm × 0.25 μm) using internal standard trimethylbenzene. The temperatures of the injector and detector were 280 °C and 250 °C, respectively. The column temperature increased from 50 °C to 280 °C at 10 °C/min and held at 280 °C for 4 min.

2.5. Calculation details

DFT calculations were implemented utilizing generalized gradient approximation (GGA) functional in the form of PBE in CASTEP package [21–24]. The convergence criterion of energy, maximum force and maximum displacement for geometry optimization was set as 1.0×10^{-5} eV/atom, 0.03 eV/Å and 0.001 Å respectively. A custom energy cutoff of 400 eV was adopted for the plane wave basis set. SCF tolerance of 1.0×10^{-6} eV/atom were applied in the computations. (101) facet of β-Mo_2C was selected as the representative surface for flavanone dehydrogenation. The periodic surface model was cleaved from bulk β-Mo_2C in a 3 × 4 supercell with nine-layer atoms using a vacuum slab with thickness of 15 Å. Top three-layer atoms in the supercell were relaxed to represent the bare surface. The k-point mesh of Brillouin zone was set to be 1 × 2 × 1 for geometry optimization and transition state search of flavanone dehydrogenation on (101) surface of β-Mo_2C. Furthermore, according to the dehydrogenation pathway of flavanone on the β-Mo_2C (101) surface, relative energies for direct dehydrogenation of flavanone without catalysis were calculated. All transition states were located by performing complete LST/QST calculations [25,26].

A layer of graphene is often employed as the simplified activated carbon model for DFT related calculations in literatures [27–29]. Considering a similar size with the β-Mo_2C (101) surface model, a two-layer graphitic carbon structure was created as the carbon material model for DFT calculations. For the B/N-doped carbon material model, atomic substitution and oxygen vacancy defect were constructed near the pre-set dehydrogenation sites to explore the possible effects of B/N doping and oxygen vacancy on flavanone dehydrogenation. For the graphitic carbon model, a 6 × 6 supercell with 15 Å thick vacuum slab was created by cleaving the (001) surface of bulk graphite and the top carbon layer was relaxed. Considering the weak interaction force between graphite layers and molecules, DFT-D correction (Grimme method) and a larger k-point density of 3 × 3 × 1 was employed to ensure successful convergences. Other calculation conditions were set the same as the β-Mo_2C (101) surface model. The constructed structures of the three carbon material models are shown in Figs. S1–S3.

3. Results and discussion

3.1. Characterization results

The Mo_2C@BNC-*x* samples were firstly characterized by XRD, as shown in Fig. 1. It is found that the typical characteristic peaks were observed at 34.4°, 37.9°, 39.5°, 52.2°, 61.7°, 69.6°, and 74.7° for Mo_2C@BNC-900 and Mo_2C@BNC-1000 samples, which belongs to the (100), (002), (101), (102), (110), (103), and (112) crystal planes of β-Mo_2C (JCPDS No. 35-0787), respectively [30,31]. Meanwhile, the Mo_2C@BNC-800 exhibited relatively weak diffraction peaks of Mo_2C nanoparticles because of the low annealing temperatures of 800 °C [32]. These results show the successful preparation of β-Mo_2C nanoparticles encapsulated in these three Mo_2C@BNC-*x* samples. Notably, the characteristic peaks of β-Mo_2C crystals were not found in the XRD patterns of Mo—N—C/1000 sample without using boric acid as the precursor material. This finding suggests that the precursor material boric acid is very essential to promote the formation of β-Mo_2C nanocrystals in the Mo_2C@BNC-*x* sample.

Fig. 2 illustrates the FTIR spectra of these three Mo_2C@BNC-*x* samples. The characteristic peaks at 1600, 1390, and 1197 cm^{-1} were discovered and assigned to the C=N stretching vibration, the in-plane B–N stretching vibration, and B—O stretching vibration [33], respectively. This indicates that boron and nitrogen elements has successfully co-doped in the Mo_2C@BNC-*x* samples. Moreover, the porosities and surface areas of Mo_2C@BNC-*x* samples were further determined by N_2 adsorption–desorption at −196 °C. It is seen from Fig. S4 that all these three Mo_2C@BNC-*x* samples displayed very low N_2 adsorption capacities. As a result, their surface areas were very small (less than 10 m^2/g), verifying the nonporosity of Mo_2C@BNC-*x* samples.

Fig. 3 displays the SEM images of Mo_2C@BNC-*x* samples. It can be seen that the primary particles of Mo_2C@BNC-800 and Mo_2-

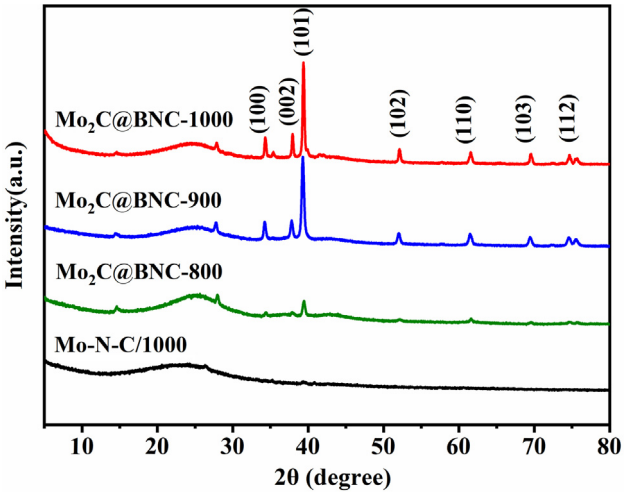

Fig. 1. XRD patterns of Mo_2C@BNC-*x* samples.

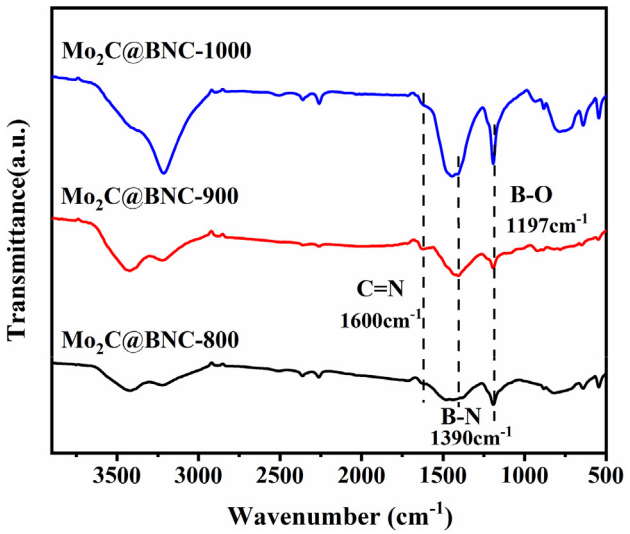

Fig. 2. FTIR spectra of Mo_2C@BNC-*x* samples.

C@BNC-900 interconnected with each other to form a very dense framework, respectively (Fig. 3A,B). As the annealing temperature further increased to 1000 °C, a uniform and loose nodular structure was obtained for Mo_2C@BNC-1000 (Fig. 3C,D). For comparison, the reference sample Mo—N—C/1000 showed a very smooth surface morphology without nodular structure (Fig. S5), which reconfirms that the precursor boric acid is essential to generate highly dispersed β-Mo_2C nanoparticles on B/N-codoped carbon frameworks. As shown in Fig. 4A, the TEM image of Mo_2C@BNC-1000 indicated that the Mo-based dots with an average size of 22.15 ± 0.68 nm were highly dispersed and encapsulated in the support B/N-codoped carbon frameworks. The HRTEM image of Mo_2C@BNC-1000 (Fig. 4B) also showed that the lattice spacing of Mo_2C was measured to be 0.23 nm, corresponding to the (1 0 1) plane of crystallized β-Mo_2C nanoparticles [34,35]. This finding reconfirmed the formation of crystallized β-Mo_2C nanoparticles in Mo_2C@BNC-1000, which agrees well with the XRD results.

The XPS measurements of Mo_2C@BNC-*x* samples were performed to analyze the elemental compositions and chemical valence states. It is shown that the Mo, C, B, N, and O elements were detected in the full-scan spectra (Fig. S6). The Mo 3d XPS spectra (Fig. 5) could be deconvoluted into three types of Mo species, corresponding to Mo^{2+} at 228.6 ± 0.2 eV, Mo^{4+} at 229.8 ± 0.1 eV, and Mo^{6+} at 232.8 ± 0.1 eV, respectively [36]. More importantly, it is found that the surface low-valence Mo^{2+} percentage in Mo_2C@BNC-1000 was greatly higher than those in Mo_2C@BNC-800 and Mo_2C@BNC-900. That is to say, the higher the carbonization temperature was, the more the content of Mo^{2+} species had. Thus, it is demonstrated that high annealing temperature can effectively induce more crystallized β-Mo_2C nanoparticles in Mo_2C@BNC-1000, which is in agreement with the XRD patterns of Mo_2C@BNC-*x*.

In addition, Fig. 6 shows the high-resolution XPS spectra of O 1s in the Mo_2C@BNC-*x* samples. It is indicated that the small deconvoluted peak located at around 530.8 eV could be associated with the lattice oxygen in Mo_2C@BNC-*x*, while the large deconvoluted peak located at around 532.4 eV was corresponding to the surface adsorption oxygen. It is believed that the proportion of the absorbed oxygen species in XPS spectra can determine the formation of surface oxygen vacancies [37]. Then the relative intensity ratio values of O 1s (adsorption oxygen)/O 1s (lattice oxygen) were calculated to be 1.67, 1.42, and 1.05, respectively, for Mo_2C@BNC-800, Mo_2C@BNC-900, and Mo_2C@BNC-1000. This suggests that increasing annealing temperature would be conducive to generate surface oxygen vacancy. In addition, EPR spectroscopy was further performed to verify oxygen vacancies on the surface of Mo_2C@BNC-*x* samples. It is seen from Fig. 7 that an obvious EPR signal at g = 2.0027 was observed for Mo_2C@BNC-1000, which is assigned to oxygen vacancies [38]. In contrast, the signal of oxygen vacancies was not detected for Mo_2C@BNC-800 and Mo_2C@BNC-900.

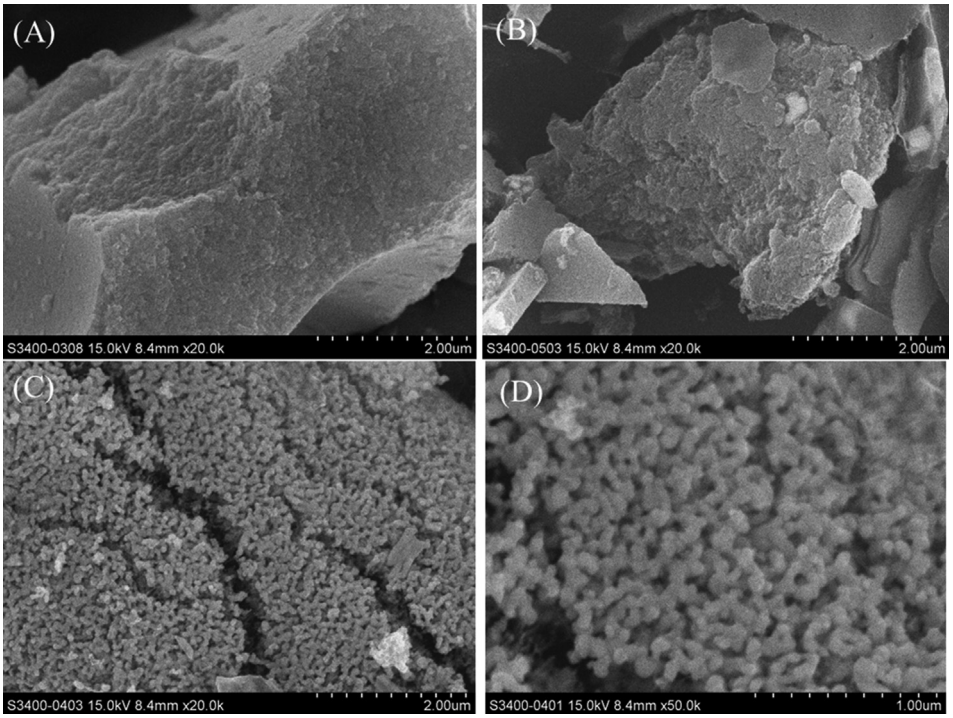

Fig. 3. SEM images of Mo_2C@BNC-800 (A), Mo_2C@BNC-900 (B), and Mo_2C@BNC-1000 (C, D).

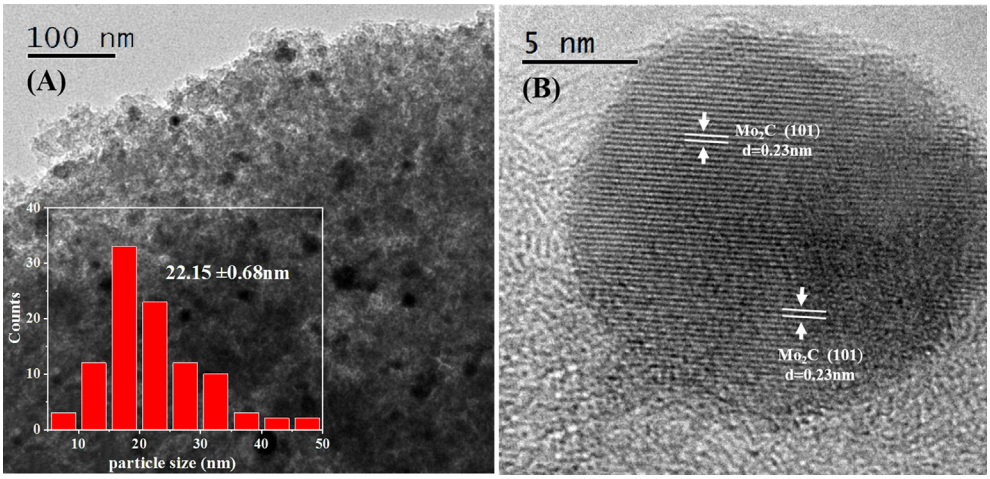

Fig. 4. TEM (A) and HRTEM (B) images of Mo_2C@BNC-1000.

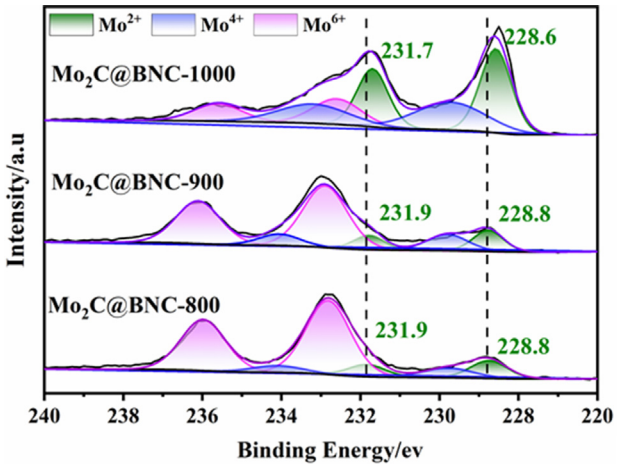

Fig. 5. XPS profiles of Mo 3d in the Mo_2C@BNC-*x* samples.

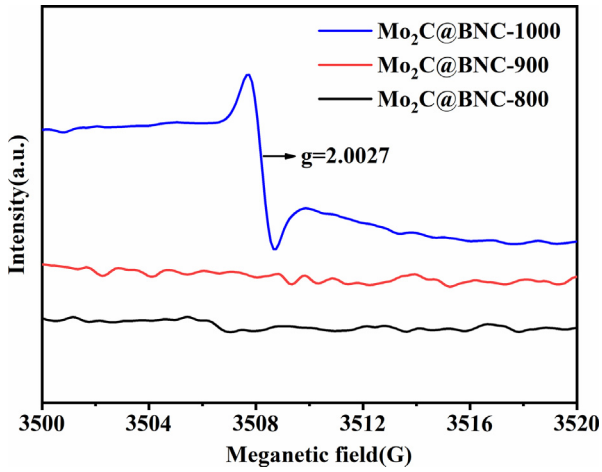

Fig. 7. EPR spectra of Mo_2C@BNC-*x* recorded at 25 °C.

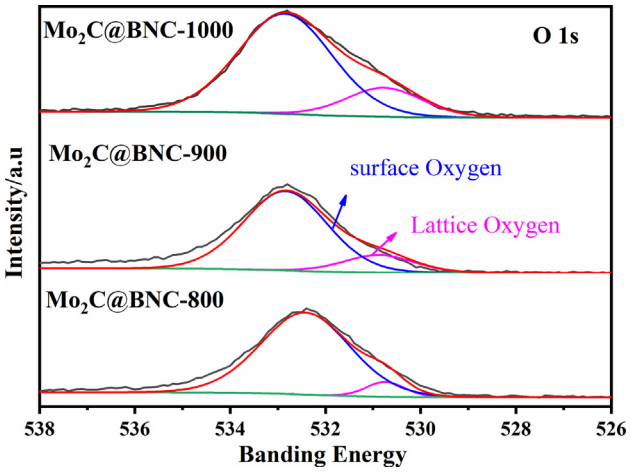

Fig. 6. XPS spectra of O 1s in the Mo_2C@BNC-*x* samples.

Therefore, it is shown that a B/N co-doped carbon supported Mo_2C catalyst incorporated with rich oxygen vacancies was successfully prepared.

3.2. Catalytic performance

The oxidative dehydrogenation of flavanones to flavones is one of the most popular procedures for the synthesis of flavones. Therefore, the as-prepared Mo_2C@BNC-*x* samples were employed

Table 1
Oxidative dehydrogenation of flavanone to flavone catalyzed by various Mo-based catalysts.

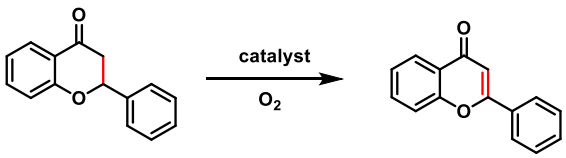

Entry	Catalyst	Conversion of flavanone	Yield of flavone
1	Mo_2C@BNC-1000	99%	99% (95%)
2	Mo_2C@BNC-900	91%	79%
3	Mo_2C@BNC-800	79%	58%
4	Mo—N—C/1000	29%	17%
5	Commercialized β-Mo_2C	10%	9%
6	β-Mo_2C/AC	15%	13%

Reaction conditions: flavanone (0.25 mmol), catalyst (0.05 g), ethanol (6 mL), 1.8 MPa O_2, 180 °C, 10 h. Value in parentheses is isolated yield.

as the catalysts in oxidative dehydrogenation of flavanone (Table 1). It is found that three Mo_2C@BNC-*x* catalysts showed different catalytic activities in oxidative dehydrogenation of flavanone to flavone under O_2 condition. The characterization results of ^1H NMR and ^{13}C NMR (Figs. S7 and S8) confirmed the successful catalytic synthesis of flavone through oxidative dehydrogenation of flavanone. The Mo_2C@BNC-1000 catalyst exhibited the best performance with a 99% conversion of flavanone and 99% yield of flavone, respectively (Table 1, entry 1). However, the other two catalysts Mo_2C@BNC-800 and Mo_2C@BNC-900 were found to have relatively low catalytic activities for oxidative dehydrogenation of flavanone to flavone, and the yields of flavone were less than 80% (Table 1, entries 2,3). Meanwhile, the reference catalyst Mo—N—C/1000 induced only 17% flavone yield (Table 1, entry 4), obviously demonstrating the key catalysis of β-Mo_2C in Mo_2-C@BNC-1000. Commercialized β-Mo_2C and activated carbon supported commercialized β-Mo_2C (β-Mo_2C/AC) were also examined to have very low yield of flavone under identical conditions (Table 1, entries 5,6), showing the importance of the support B/N-codoped carbon in the oxidation reaction of flavone.

Furthermore, the effect of reaction parameters such as solvent, temperature, and time on the yield of flavone was studied in detail. First, optimization of the reaction solvent indicated that strong polar solvents had a positive impact on the oxidative dehydrogenation of flavanone to flavone. The highest flavone yield of 99% could be obtained in ethanol at 180 °C and 10 h (Table S1). However, the low-polar solvent toluene induced only 62% yield of flavone. Moreover, as shown in Fig. S9a, it is demonstrated that the oxidative dehydrogenation of flavanone to flavone was obviously accelerated by the increase of reaction temperature from 150 to 180 °C. However, no apparent increases in the conversion of flavanone and yield of flavone were observed at 190 °C. Thus, the optimal temperature of 180 °C was chosen in the following experiments. In addition, Fig. S9b shows the time-dependent catalytic performance of Mo_2C@BNC-1000 for oxidative dehydrogenation of flavanone to flavone at 180 °C. Both the conversion of flavanone and the yield of flavone could greatly enhance from 4 h to 10 h. The flavanone was found to be almost completely oxidized into flavone at 10 h. After screening of the reaction conditions, the optimized parameters were set as follows: Mo_2C@BNC-1000 as the catalyst, ethanol as the solvent, O_2 as the oxidant, temperature of 180 °C, and reaction time of 10 h.

Inspired by the above-mentioned promising results, the comparison results of oxidative dehydrogenation of flavanone to flavone catalyzed by Mo_2C@BNC-1000 and other reported catalysts were summarized and listed in Table S2. It can be seen that Mo_2-C@BNC-1000 showed excellent catalytic activity for highly efficient synthesis of flavone, which is much better than the performance of heterogeneous gold catalyst Au/LDH [6]. Moreover, the previous homogeneous catalysis systems for oxidative dehydrogenation of flavanone to flavone relied on using an unwelcoming I_2 as the oxidant or adding a relatively expensive ionic liquid as the solvent [4,5]. These progresses are still inferior to the performance of Mo_2-C@BNC-1000 catalyst. Therefore, Mo_2C@BNC-1000 is considered to be the outstanding non-noble metal heterogeneous catalyst for highly efficient oxidative dehydrogenation of flavanone to flavone under mild conditions (Scheme 1).

3.3. Reactive oxygen species

In order to further investigate whether reactive oxygen species were generated in the oxidative dehydrogenation of flavanone, the active species trapping experiments were carried out by using various radical scavengers. As shown in Table 2, both the conversion of flavanone and yield of flavone decreased significantly by adding free radical scavenger butylated hydroxytoluene (Table 2, entry 2), implying that the oxidative dehydrogenation of flavanone involves a free radical process. Meanwhile, this reaction was inhibited obviously by adding hydroxyl radical scavenger tertiary butanol (Table 2, entry 3). This suggests that the hydroxyl radicals would be the reactive oxidative species. In contrast, no obvious decrease in the conversion of flavanone and yield of flavone were observed, when the superoxide radical quencher 1,4-benzoquinone and hole scavenger ammonium formate were added, respectively (Table 2, entries 4,5).

Subsequently, EPR spin-trapping was used to directly test oxygen species in oxidative dehydrogenation reaction of flavanone. It can be seen from Fig. 8 that four characteristic peaks of ·DMPO-OH adducts (sign ■) with an intensity ratio of 1:2:2:1 were clearly detected [39,40], offering conclusive evidence for the generation of ·OH radicals. Moreover, a strong six lines hyperfine pattern (sign ○) was observed and identified as the ·DMPO-CH_3 spin adduct generated as result of the interaction between the ·OH free radical with the solvent ethanol [40]. A three-line DMPOX signal (sign ◆) was also detected derived from the decomposition of DMPO to an oxidized form DMPOX [39,41]. Therefore, it is demonstrated that the Mo_2C@BNC-1000 catalyst possessing rich oxygen vacancies has a good ability to activate molecular oxygen. The oxygen vacancies in Mo_2C@BNC-1000 could boost electron localization and charge separation and promote the generation of more hydroxyl radicals smoothly, which results in the best catalytic performance for oxidative dehydrogenation of flavanone.

3.4. Oxidative dehydrogenation mechanism

To understand the reaction mechanism in more detail, the dehydrogenation pathway of flavanone was investigated by DFT calculations. Energy changes of catalytic dehydrogenation of flavanone on β-Mo_2C (101) surface and its direct dehydrogenation without catalysis with the same dehydrogenation sequence are represented in Fig. 9. The optimized structures of different chemical states during DFT calculations are displayed in Figs. S10 and S11. As well known, the dehydrogenation reaction is generally endothermic. It can be obviously observed the direct dehydrogenation of flavanone needs to cross particularly high energy barriers. The total reaction energy for flavanone into flavone is a s high as 6.80 eV without catalysis, which is only 0.40 eV on β-Mo_2C (101) surface. In detail, removing the first H atom requires 4.43 eV for transition state TS1, while the activation barrier to overcome on β-Mo_2C (101) surface is only 1.27 eV. Similarly, the energy barrier (TS2) to deprive the second H atom directly is 2.6 eV which is 0.55 eV higher than that needed on β-Mo_2C (101) surface. In particular, $C_{15}H_{11}O_2$* is unstable on β-Mo_2C (101) surface, easy to further lose another H atom to form the more stable $C_{15}H_{10}O_2$* and release an energy of 0.6 eV. While, the reaction energy for $C_{15}H_{11}O_2$* to generate the free $C_{15}H_{10}O_2$ is as high as +4.48 eV, which is −0.4 eV on β-Mo_2C (101) surface, further indicating the dehydrogenation reaction is difficult to carry out without catalyst. It can be conclude that the overwhelming energy barrier for dehydrogenation of flavanone is greatly reduced on β-Mo_2C.

Above analysis has demonstrated that β-Mo_2C can greatly reduce the activation energy of flavanone dehydrogenation. However, it is still remained uncertainty whether the B/N doped carbon materials possess the same property as β-Mo_2C demonstrating. In order to investigate the behavior of flavanone on B/N-doped carbon materials, the adsorption and subsequent dehydrogenation of flavanone on the surface of B/N-doped carbon materials was planned to carry calculation. Considering the existing possible inhomogeneity of B/N doping on the surface of carbon materials, three models with different surface structures were constructed: the carbon material without B/N doping, the carbon material doped with B/N and the B/N-doped carbon material with O

Table 2
Active species trapping experiments for oxidative dehydrogenation of flavanone.

Entry	Quencher	Quenching group	Conversion of flavanone	Yield of flavone
1	–	–	99%	99%
2	Butylated hydroxytoluene	Free radicals	10%	10%
3	Tertiary butanol	·OH	5%	3%
4	1,4-benzoquinone	$\cdot O_2^-$	99%	99%
5	Ammonium formate	Hole	95%	90%

Reaction conditions: flavanone (0.25 mmol), catalyst (0.05 g), ethanol (6 mL), 1.8 MPa O_2, 180 °C, 10 h. The amount of quencher is 0.025 mmol.

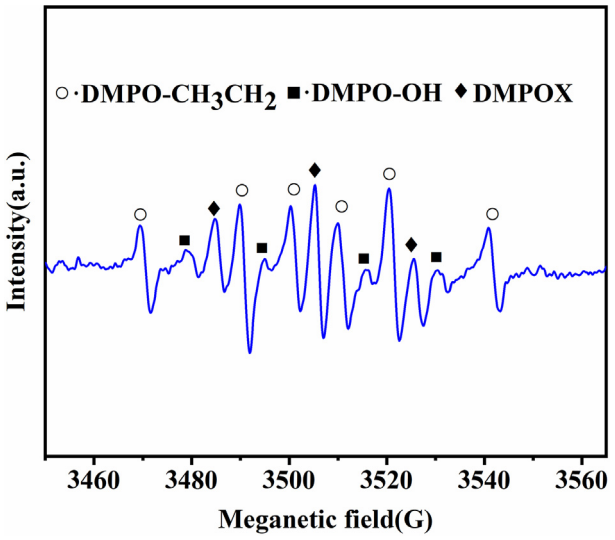

Fig. 8. The DMPO spin-trapping EPR spectra for free radical in the catalytic mixture of flavanone, O_2, solvent ethanol, and catalyst Mo_2C@BNC-1000 at 25 °C.

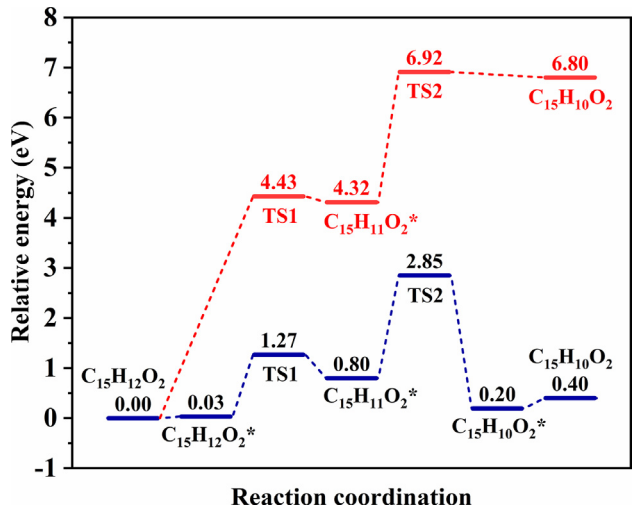

Fig. 9. Relative energy profiles of flavanone dehydrogenation on β-Mo_2C (101) surface (route in dark blue) and its direct dehydrogenation without catalysis (route in red). (For interpretation of the references to colour in this figure legend, the reader is referred to the web version of this article.)

vacancy on the surface. These constructed models are shown in Figs. S12–S14. At the beginning when calculating the dehydrogenation of flavanone on carbon materials, it is surprisingly found that flavanones are difficult to adsorb on the surface of these three carbon material models. Obvious repulsion was observed between flavanone molecule and the surface of above carbon materials, as shown in Movies S1-S3, indicating that it is difficult for flavanone molecule to effectively adsorb on the carbon material surface and go through subsequent molecule dissociation. In the calculating procedure, even manually deprive an active H on the flavanone away from the flavanone molecule and place it on the surface of the carbon material in the initial structure setting, the $^*C_{15}H_{11}O_2$ that losing the H atom would still move far away from the surface of the material after optimization. Even if the flavanone loses an active hydrogen, the surface of the carbon material still repel it. At the same time, $^*C_{15}H_{11}O_2$ will attract the H atoms that are forcibly pulled out, which indicates that it is difficult for flavanones to dissociate and dehydrogenate on the surface. It is likely that the two large benzene rings in the flavanone molecule are mutually repelled with the benzene ring-like structure of the carbon materials, which is similar to that there is always a large distance between the top and bottom graphite layers.

The DFT results have proved it is almost impossible for flavanone dehydrogenation on bare surface of B/N-doped carbon materials and β-Mo_2C can largely reduce the energy barriers for the dehydrogenation procedure. The oxidative dehydrogenation of flavanone consists of dehydrogenation and oxidation of the dissociated H atoms. In former characterization, it has been demonstrated that there are abundant oxygen vacancies on Mo_2C@BNC-1000 which has a good ability to activate molecular oxygen to produce rich hydrogen acceptors. Particularly, the carbon material is an excellent promotor to accelerate hydrogen spillover [42,43], in which case fast bridges would be built between oxygen vacancies and β-Mo_2C sites. The hydrogen atoms sourced from flavanone dehydrogenation on β-Mo_2C can efficiently migrate to molecular oxygen with the generation of hydroxyl radicals and favor the oxidative dehydrogenation progress of flavanone. These synergistic effects might be the reason why the catalyst Mo_2C@BNC-1000 can efficiently catalyze the oxidative dehydrogenation of flavanones.

3.5. Applicability and reusability of Mo_2C@BNC-1000

The oxidative dehydrogenation of flavanone derivatives with different substituting groups was further conducted to study the applicability of the Mo_2C@BNC-1000 catalyst. As shown in Table 3, it is found that various flavanones bearing electron-donating and electron-withdrawing groups could be converted to the corresponding substituted flavones with high yields of 70–99%. For example, the electron-donating-OCH_3 group afforded the corresponding substituted flavanone in 95–99% yields. However, the electron-withdrawing effect of —Cl group had a slightly negative impact on the oxidation reaction, which gives only 70% yield of —Cl group substituted flavone. Finally, the reusability of the Mo_2C@BNC-1000 catalyst was explored. As shown in Fig. 10, no obvious decline in flavanone conversion and flavone yield was observed after 5 successive cycles, indicating good stability of Mo_2C@BNC-1000 under optimized reaction condition. Moreover, compared with the fresh catalyst, the XRD patterns of the regenerated Mo_2C@BNC-1000 catalyst showed the well preserved diffraction peaks of β-Mo_2C nanoparticles (Fig. S15). Also, TEM characterization results of reused Mo_2C@BNC-1000 catalyst (Fig. S16) further

Table 3
Oxidative dehydrogenation of various flavanones catalyzed by Mo_2C@BNC-1000.

Entry	Substrate	Product	Conversion	Yield
1	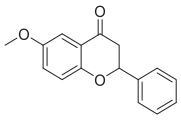	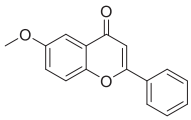	99%	99%
2	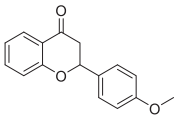	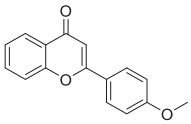	98%	95%
3	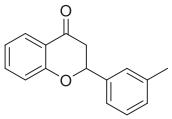	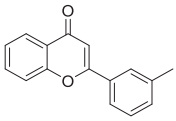	85%	80%
4	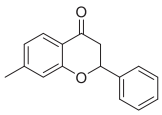	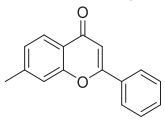	88%	85%
5	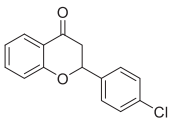	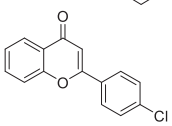	70%	70%

Reaction conditions: substrate (0.25 mmol), catalyst (0.05 g), ethanol (6 mL), 1.8 MPa O_2, 180 °C, 10 h.

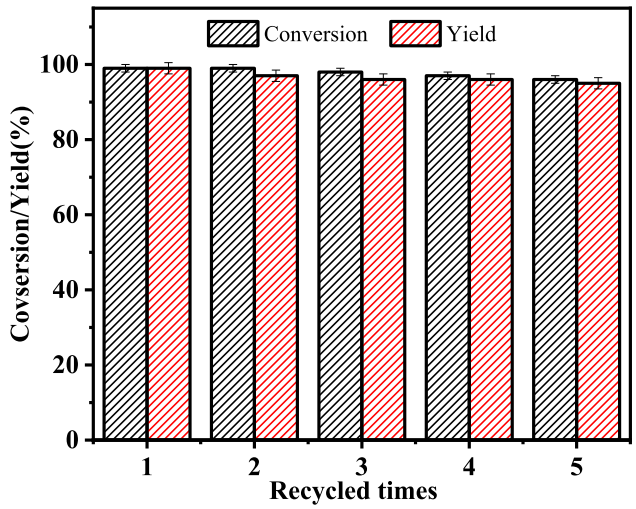

Fig. 10. Reusability of the Mo_2C@BNC-1000 catalyst in oxidative dehydrogenation of flavanone to flavone.

demonstrated that the catalyst had no obvious change in structure and morphology even used for up to 5 cycles.

4. Conclusions

In this work, a series of Mo_2C@BNC-*x* catalysts was successfully prepared using phosphomolybdic acid, urea, boric acid, and glucose as precursors through a simple and effective one-step pyrolysis method. It is found that the as-prepared Mo_2C@BNC-1000 catalyst displayed outstanding catalytic activity and stability toward oxidative dehydrogenation of flavanones into flavones. Several characterizations and DFT calculations demonstrated β-Mo_2C could greatly reduce the activation energy of flavanone dehydrogenation, and simultaneously abundant oxygen vacancies on Mo_2C@BNC-1000 could activate molecular oxygen binding with the dissociated H atoms to generate hydroxyl radicals for accelerating hydrogen spillover. The synergistic effect between Mo_2C and the B,N-codoped carbon material with rich oxygen vacancies on Mo_2C@BNC-1000 was thus considered to account for the excellent performance in the oxidative dehydrogenation of flavanones. This work presents an outstanding non-noble metal heterogeneous catalyst for highly efficient synthesis of flavones through oxidative dehydrogenation.

CRediT authorship contribution statement

Wen-Ting Chen: Investigation, Writing – original draft, Data curation. **Song Han:** Methodology, Investigation. **Zi-Teng Gao:** Methodology, Investigation. **Ming-Shuai Sun:** Methodology, Investigation, Writing – review & editing. **Zhang-Min Li:** Funding acquisition, Methodology, Writing – review & editing. **Duan-Jian Tao:** Supervision, Conceptualization, Funding acquisition, Resources, Writing – review & editing.

Declaration of Competing Interest

The authors declare that they have no known competing financial interests or personal relationships that could have appeared to influence the work reported in this paper.

Acknowledgments

We gratefully thank the Key Research and Development Program of Jiangxi Province (20202BBGL73118) and the National Natural Science Foundations of China (22068013) for financial support. W.T. Chen thanks the Scientific Research Foundation of graduate innovation of Jiangxi Province Education Department (YC2021-B064) for her financial support.

Appendix A. Supplementary material

Supplementary data to this article can be found online at https://doi.org/10.1016/j.jcis.2022.05.081.

References

[1] L. Cruz, N. Basílio, N. Mateus, V. de Freitas, F. Pina, Natural and synthetic flavylium-based dyes: the chemistry behind the color, Chem. Rev. 122 (1) (2022) 1416–1481.

[2] H. Zhang, G. Xie, M. Tian, Q. Pu, M. Qin, Optimization of the ultrasonic-assisted extraction of bioactive flavonoids from ampelopsis grossedentata and subsequent separation and purification of two flavonoid aglycones by high-speed counter-current chromatography, Molecules 21 (2016) 1096.

[3] Y.-Y. Zhang, H. Li, X. Jiang, C.V. Subba Reddy, H. Liang, Y. Zhang, R. Cao, R.-Y. Sun, M.K. Tse, L. Qiu, Nickel-catalyzed decarbonylative cycloaddition of benzofuran-2,3-diones with alkynes to flavones, Adv. Synth. Catal. 364 (3) (2022) 525–530.

[4] M.M. Naik, S.G. Tilve, V.P. Kamat, Pyrrolidine and iodine catalyzed domino aldol-Michael-dehydrogenative synthesis of flavones, Tetrahedron Lett. 55 (22) (2014) 3340–3343.

[5] Z. Du, H. Ng, K. Zhang, H. Zeng, J. Wang, Ionic liquid mediated Cu-catalyzed cascade oxa-Michael-oxidation: efficient synthesis of flavones under mild reaction conditions, Org. Biomol. Chem. 9 (2011) 6930–6933.

[6] T. Yatabe, X. Jin, K. Yamaguchi, N. Mizuno, Gold nanoparticles supported on a layered double hydroxide as efficient catalysts for the one-pot synthesis of flavones, Angew. Chem. Int. Ed. 54 (45) (2015) 13302–13306.

[7] J.R. Kitchin, J.K. Nørskov, M.A. Barteau, J.G. Chen, Trends in the chemical properties of early transition metal carbide surfaces: a density functional study, Catal. Today 105 (1) (2005) 66–73.

[8] R.B. Levy, M. Boudart, Platinum-like behavior of tungsten carbide in surface catalysis, Science 181 (4099) (1973) 547–549.

[9] H. Sun, G. Li, J. Luo, M. Rao, Z. Peng, T. Jiang, Thermodynamics guided ultrafast and continuous preparation of Mo_2C nanocrystals for hydrogen evolution electrocatalysis, Mater. Des. 193 (2020) 108803.

[10] Z. Li, C. Chen, E. Zhan, N.a. Ta, Y. Li, W. Shen, Crystal-phase control of molybdenum carbide nanobelts for dehydrogenation of benzyl alcohol, Chem. Commun. 50 (34) (2014) 4469.

[11] E. Gomez, B. Yan, S. Kattel, J.G. Chen, Carbon dioxide reduction in tandem with light-alkane dehydrogenation, Nat. Rev. Chem. 3 (11) (2019) 638–649.

[12] Q. Gao, W. Zhang, Z. Shi, L. Yang, Y. Tang, Structural design and electronic modulation of transition-metal-carbide electrocatalysts toward efficient hydrogen evolution, Adv. Mater. 31 (2019) 1802880.

[13] W.-J. Kwak, K.C. Lau, C.-D. Shin, K. Amine, L.A. Curtiss, Y.-K. Sun, A Mo_2C/Carbon nanotube composite cathode for lithium–oxygen batteries with high energy efficiency and long cycle life, ACS Nano 9 (4) (2015) 4129–4137.

[14] Y. Ma, G. Guan, X. Hao, J.i. Cao, A. Abudula, Molybdenum carbide as alternative catalyst for hydrogen production–a review, Renew. Sust. Energy Rev. 75 (2017) 1101–1129.

[15] Y. Xu, R. Wang, J. Wang, J. Li, T. Jiao, Z. Liu, Facile fabrication of molybdenum compounds (Mo_2C, MoP and MoS_2) nanoclusters supported on N-doped reduced graphene oxide for highly efficient hydrogen evolution reaction over broad pH range, Chem. Eng. J. 417 (2021) 129233.

[16] X. Zhang, X. Dai, K.-H. Wu, B. Su, J. Chen, W. Qi, Z. Xie, A generalized approach to adjust the catalytic activity of borocarbonitride for alkane oxidative dehydrogenation reactions, J. Catal. 405 (2022) 105–115.

[17] L. Wang, C. Wang, Z. Zhang, J. Wu, R. Ding, B. Lv, Thermal induced BCN nanosheets evolution and its usage as metal-free catalyst in ethylbenzene dehydrogenation, Appl. Surf. Sci. 422 (2017) 574–581.

[18] J. Sheng, B. Yan, W.-D. Lu, B. Qiu, X.-Q. Gao, D. Wang, A.-H. Lu, Oxidative dehydrogenation of light alkanes to olefins on metal-free catalysts, Chem. Soc. Rev. 50 (2) (2021) 1438–1468.

[19] Y. Chen, L. Fu, Z. Liu, Y. Wang, Ionic-liquid-derived boron-doped cobalt-coordinating nitrogen-doped carbon materials for enhanced catalytic activity, ChemCatChem 8 (10) (2016) 1782–1787.

[20] R. Goyal, B. Sarkar, A. Bag, F. Lefebvre, S. Sameer, C. Pendem, A. Bordoloi, Single-step synthesis of hierarchical BxCN: a metal-free catalyst for low-temperature oxidative dehydrogenation of propane, J. Mater. Chem. A 4 (2016) 18559–18569.

[21] S.J. Clark, M.D. Segall, C.J. Pickard, P.J. Hasnip, M.I.J. Probert, K. Refson, M.C. Payne, First principles methods using CASTEP, Z. Kristallogr. 220 (2005) 567–570.

[22] W. Kohn, L.J. Sham, Self-consistent equations including exchange and correlation effects, Phys. Rev. 140 (4A) (1965) A1133–A1138.

[23] J.P. Perdew, K. Burke, M. Ernzerhof, Generalized gradient approximation made simple, Phys. Rev. Lett. 77 (18) (1996) 3865–3868.

[24] G. Kresse, D. Joubert, From ultrasoft pseudopotentials to the projector augmented-wave method, Phys. Rev. B 59 (3) (1999) 1758–1775.

[25] T.A. Halgren, W.N. Lipscomb, The synchronous-transit method for determining reaction pathways and locating molecular transition states, Chem. Phys. Lett. 49 (2) (1977) 225–232.

[26] N. Govind, M. Petersen, G. Fitzgerald, D. King-Smith, J. Andzelm, A generalized synchronous transit method for transition state location, J. Com. Mat. Sci. 28 (2) (2003) 250–258.

[27] K.e. Zhou, W. Ma, Z. Zeng, X. Ma, X. Xu, Y. Guo, H. Li, L. Li, Experimental and DFT study on the adsorption of VOCs on activated carbon/metal oxides composites, Chem. Eng. J. 372 (2019) 1122–1133.

[28] M. Wei, F. Marrakchi, C. Yuan, X. Cheng, D. Jiang, F.F. Zafar, Y. Fu, S. Wang, Adsorption modeling, thermodynamics, and DFT simulation of tetracycline onto mesoporous and high-surface-area NaOH-activated macroalgae carbon, J. Hazard. Mater.127887 425 (2022).

[29] X. Liu, Y. Han, Y. Cheng, G. Xu, Microwave-assisted ammonia modification of activated carbon for effective removal of phenol from wastewater: DFT and experiment study, Appl. Surf. Sci. 518 (2020) 146258.

[30] H. Lin, N. Liu, Z. Shi, Y. Guo, Y.i. Tang, Q. Gao, Cobalt-doping in molybdenum-carbide nanowires toward efficient electrocatalytic hydrogen evolution, Adv. Funct. Mater. 26 (31) (2016) 5590–5598.

[31] J. Jia, T. Xiong, L. Zhao, F. Wang, H. Liu, R. Hu, J. Zhou, W. Zhou, S. Chen, Ultrathin N-doped Mo_2C nanosheets with exposed active sites as efficient electrocatalyst for hydrogen evolution reactions, ACS Nano 11 (12) (2017) 12509–12518.

[32] Q.-C. Zhu, S.-M. Xu, M.M. Harris, C. Ma, Y.-S. Liu, X. Wei, H.-S. Xu, Y.-X. Zhou, Y.-C. Cao, K.-X. Wang, J.-S. Chen, A composite of carbon-wrapped Mo_2C nanoparticle and carbon nanotube formed directly on Ni foam as a high-performance binder-free cathode for Li-O_2 batteries, Adv. Funct. Mater. 26 (46) (2016) 8514–8520.

[33] J. Sheng, B. Yan, B. He, W.-D. Lu, W.-C. Li, A.-H. Lu, Nonmetallic boron nitride embedded graphitic carbon catalyst for oxidative dehydrogenation of ethylbenzene, Catal. Sci. Technol. 10 (6) (2020) 1809–1815.

[34] J. Dong, Y. Shi, C. Huang, Q. Wu, T. Zeng, W. Yao, A new and stable Mo-Mo_2C modified g-C_3N_4 photocatalyst for efficient visible light photocatalytic H_2 production, Appl. Catal. B: Environ. 243 (2019) 27–35.

[35] Y. Liu, G. Yu, G.-D. Li, Y. Sun, T. Asefa, W. Chen, X. Zou, Coupling Mo_2C with nitrogen-rich nanocarbon leads to efficient hydrogen-evolution electrocatalytic sites, Angew. Chem. Int. Ed. 54 (37) (2015) 10752–10757.

[36] W. Cui, N. Cheng, Q. Liu, C. Ge, A.M. Asiri, X. Sun, Mo_2C nanoparticles decorated graphitic carbon sheets: biopolymer-derived solid-state synthesis and application as an efficient electrocatalyst for hydrogen generation, ACS Catal. 4 (2014) 2658–2661.

[37] C. Yu, S. Yu, L. Li, Upgraded methyl oleate to diesel-like hydrocarbons through selective hydrodeoxygenation over Mo-based catalyst, Fuel 308 (2022) 122038.

[38] Q. Zhang, X. Zhao, L. Duan, H. Shen, R. Liu, T. Hou, Optical and photocatalytic properties of a ZnO@C core/shell sphere with rich oxygen vacancies, CrystEngComm 22 (31) (2020) 5245–5254.

[39] B. Aguilera-Venegas, C. Olea-Azar, V.J. Aran, J.D. Maya, U. Kemmerling, H. Speisky, F. Mendizabal, Electrochemical, ESR and theoretical insights into the free radical generation by 1,1'-hydrocarbylenebisindazoles and its evaluation as potential bio-active compounds, Int. J. Electrochem. Sci. 7 (2012) 5837–5863.

[40] Z. Song, W. Huang, Y. Zhou, Z.-Q. Tian, Z.-M. Li, D.-J. Tao, Thermally regulated molybdate-based ionic liquids toward molecular oxygen activation for one-pot oxidative cascade catalysis, Green Chem. 22 (1) (2020) 103–109.

[41] A. Lawrence, C.M. Jones, P. Wardman, M.J. Burkitt, Evidence for the role of a peroxidase compound I-type intermediate in the oxidation of glutathione, NADH, ascorbate, and dichlorofluorescin by cytochrome c/H2O2. Implications for oxidative stress during apoptosis, J. Biol. Chem. 278 (32) (2003) 29410–29419.

[42] M. Boudart, A.W. Aldag, M.A. Vannice, On the slow uptake of hydrogen by platinized carbon, J. Catal. 18 (1970) 46–51.

[43] L. Chen, A.C. Cooper, G.P. Pez, H. Cheng, Mechanistic study on hydrogen spillover onto graphitic carbon Materials, J. Phys. Chem. C 111 (51) (2007) 18995–19000.